Paper Technology

Patrick Wegele and L. Daniel Söderberg*

On the influence of macro-scale stress variations on the dynamic dewatering of water-saturated polymer fibre networks

https://doi.org/10.1515/npprj-2025-0015 Received March 14, 2025; accepted May 4, 2025; published online June 17, 2025

Abstract: Efficient mechanical dewatering in paper manufacturing is essential for reducing energy consumption and enhancing operational efficiency. Practical observations indicate that press felt and roll cover structures significantly influence dewatering performance. While previous studies have focused on micro-scale stress variations at the paper web-press felt interface, this study extends the analysis to the press felt-roll cover interface. Using a custom dynamic compression setup, we investigate how different groove patterns impact press felt dewatering. The results show that macro-scale stress variations play a crucial role, with controlled mechanical inhomogeneities enhancing felt permeability. Through multivariate regression analysis, an optimized groove pattern is identified that improves dewatering by approximately 7% under highly dynamic pressing conditions. These findings offer valuable insights into optimizing press felt and roll cover interactions, providing a methodology to enhance nip dewatering efficiency. The study highlights the need to tailor groove patterns to specific press felts to ensure optimal water flow under saturated conditions. This research contributes to improving paper machine performance by maximizing water removal while reducing energy consumption, supporting both economic and environmental sustainability in the industry.

Keywords: mechanical dewatering; optimization; permeability; stress variations

1 Introduction

Due to its strong influence on the energy consumption of sheet drying in a paper machine, efficient wet pressing is a key lever to increase the economic and ecological efficiency. Besides process parameters like dwell time and peak pressure, multiple investigations show that the used press felt surface has a substantial impact on the overall dewatering process efficiency (e.g. Fekete 1975; Gullbrand and Vomhoff 2003; l'Anson and Ashwort 2000; McDonald and Pikulik 1992; Oliver and Wiseman 1977; Sze 1986). Its effects also depend on the amount of water that needs to be removed; as for high paper grammages, a coarser felt surface structure provides higher mechanical dewatering (McDonald et al. 2002; Sze 1986). Even though these effects were known, they were first explained in depth by Vomhoff and Norman (1997) by acknowledging the existence of an interface layer in the paper web, which is created when batt fibres of the press felt impede micro-scale stress variations in the paper web. As a result, uncompressed and highly permeable areas exist in the paper web, enhancing the overall web dewatering especially for higher grammages. Consequently, Gullbrand and Vomhoff (2005) defined a transition grammage for the paper web, describing the necessary batt fibre structure to achieve optimized paper web dewatering.

Modern paper machines employ grooved roll covers to provide additional void space for water expelled from the paper web and press felt, thereby enhancing press performance (Skelton and Toney 1998). As depicted in Figure 1, structured roll covers induce macro-scale stress variations on the backside of the press felt, creating regions of locally reduced porosity above the land areas. Since porosity is a key determinant of the resulting permeability in press felts (e.g. Ballard 1986; Chevallier 1992; Kershaw 1972; Machlem 1961; Thibault and Bloch 2008; Thibault et al. 2001), variations in compression lead to local permeability differences, resulting in a two-dimensional (2D) permeability field as a function of both the cross-machine direction (CD) and the thickness (z-direction). Consequently and in contrast to what is assumed for the paper web (Vomhoff 2000), the flow through the press felt into the grooves of a roll cover exhibits both

^{*}Corresponding author: L. Daniel Söderberg, Department of Fibre and Polymer Technology, KTH Royal Institute of Technology, Teknikringen 56, Stockholm, SE-100 44, Sweden, E-mail: dansod@kth.se. https://orcid.org/0000-0003-3737-0091

Patrick Wegele, Department of Fibre and Polymer Technology, KTH Royal Institute of Technology, Teknikringen 56, Stockholm, SE-100 44, Sweden; and J.M. Voith SE & Co. KG, St. Pöltener Straße 43, Heidenheim an der Brenz 89522, Germany

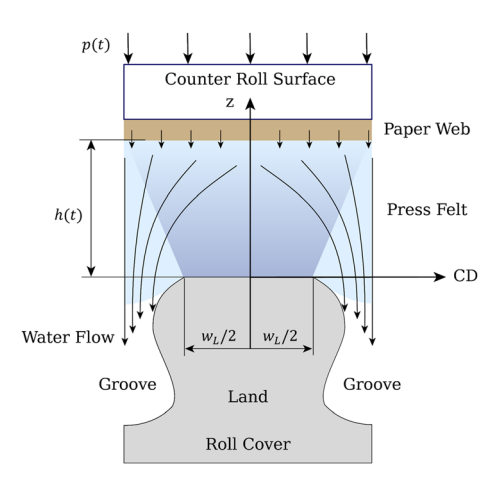


Figure 1: The hypothesis of inhomogeneous compression of a press felt by a deforming grooved roll cover, which causes varying 2D-permeability field in the press felt that generates a flow with in-plane and out-of-plane components into the grooves of the roll cover. With higher felt compression (deeper blue colour), a low local porosity in the press felt is created, causing a low local permeability to be established.

out-of-plane and in-plane components (Thibault and Bloch 2008; Thibault et al. 2001), which are caused by a deflection of the transversal flow into the grooves of the roll cover. Given this anisotropy in permeability, we postulate that the specific combination of the press felt and roll cover groove pattern strongly influences the press felt dewatering.

To classify stress variations in the press felt at different scales, we follow the definition given by MacGregor (1989) that macro-scale stress variations are caused by the base layer of the felt or the grooves of a roll cover and are in the range of 0.5-2 mm. In contrast, micro-scale stress variations are caused by individual batt fibres, which are in a range of 10 to 80 µm (Gullbrand and Vomhoff 2005; Xu et al. 2011). While extensive research has been conducted on micro-scale stress variations, less is reported on the impact of macroscale stress variations on the dynamic dewatering properties of fibre networks. Moreover, several experimental studies conducted at both industrial and pilot scales suggest that macro-scale stress variations significantly influence the overall dewatering efficiency of the pressing process (Armstrong 2005; Xu et al. 2011, 2013). To further elucidate these effects, this study investigates the influence of macro-scale stress variations on press felt dewatering. Specifically, we aim to address the following key research questions:

- Do macro-scale stress variations influence the dynamic dewatering of saturated fibre networks?
- Is an even pressure distribution or the generation of local low-resistance flow paths beneficial for optimized press felt dewatering?
- Can groove patterns be tailored to optimize the dewatering efficiency for specific press felts?

The objective of this study is thus to provide a detailed understanding of the dynamic dewatering and the possibilities for optimization within the press nip, extending the findings of Vomhoff and colleagues (Gullbrand and Vomhoff 2003, 2005; Vomhoff and Norman 1997) from the paper web-press felt interface to the press felt-roll cover interface.

2 Materials and methods

2.1 Mechanical setup and procedure

To address the scientific questions, we employed a custom experimental setup, as shown in Figure 2. A press felt sample $(35 \times 45 \, \text{mm})$ with known water content close to full saturation was placed on a carrier between an impact body and a target body, held by a scissors mechanism. Differently structured inserts manufactured from stainless steel were mounted on the target body to simulate different groove patterns. During the experiment, the impact body was lowered, simulating the dynamics of a press nip and the compression of the press felt. While the displacement of the press felt was continuously recorded using eddy current sensors (Type DT3005-S2, Micro-Epsilon), a 25 kN load cell was used to determine the corresponding load. Following the compression impulse, the target body was rapidly lifted with the intent of immediate separation of the press felt from the grooved insert. The goal of this is to, as far as possible, prevent backflow of water from the grooves into the sample, commonly known as "rewetting." The dewatering achieved during an individual experiment was obtained by measuring the sample mass before and after the impulse with a precision scale (Type Kern & Sohn ABJ 220-4M, $d = 0.1 \,\mathrm{mg}$). The entire setup was integrated into a servohydraulic testing machine (MTS 858, MTS Systems), allowing for controlling the applied load rate $\dot{\sigma}$ and load σ . The press felt used in this study is depicted in Figure 2. It consists of a double-layer base layer with monofilaments ($d = 390 \, \mu m$) and multifilaments ($d = 200 \mu m$) in cross direction (CD) and monofilaments in machine direction (MD). On the paper side, two batt fibre layers with 39 μm (first layer) and 63 μm (second layer) are present, while further batt fibre layers with identical fibre sizes are used on the backing side. The press felt has a total grammage of $w_f = 1,480 \text{ g/m}^2$, a saturation grammage of $w_s = 2,700 \text{ g/m}^2$, a porosity of $\phi_0 = 0.358 \text{ and}$ is industrially used in applications where nip dewatering is desired.

To investigate the influence of the macro-scale stress variations on the dynamic dewatering behaviour of the press felt, it was compressed against three different patterns, A, B,

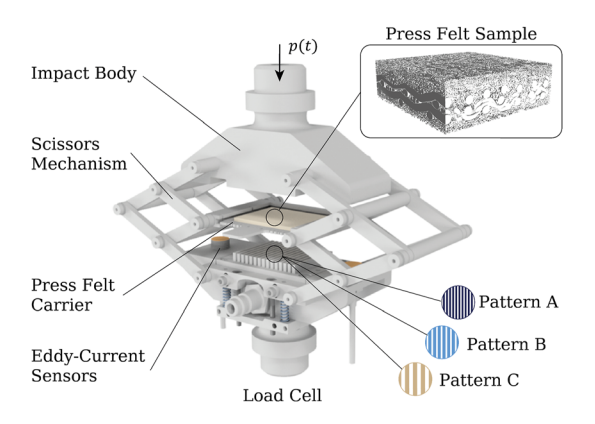


Figure 2: The setup used to perform the press felt compression and dewatering experiments. The press felt is placed in the carrier. As the impact body moves downwards, the press felt gets pressed against the grooved inserts and removed immediately after the press impulse again. Eddy-current sensors on the sides record the displacement of the press felt during the impulse. Different groove inserts allow the investigation of the compression properties of press felt samples compressed against different counter surfaces.

and C, simulating the structure of grooved roll covers used in industrial paper machines. The detailed geometrical parameters of these groove patterns are provided in Table 1. Special attention was given to maintaining a constant open area across all patterns, ensuring the absolute pressure on the land areas to remained consistent. The depth of the grooves is chosen so that the void volume in the grooves exceeds the void volume in the press felt, which prevents the creation of a hydraulic counterpressure in the grooves due to filling with expelled water.

2.2 Experimental procedure

The driving force for the flow through a fibre network is the hydraulic pressure, while the structural pressure accounts for the consolidation of the structure. Since the generated hydraulic pressure depends on the compression speed of

Table 1: Geometry of the groove inserts used in the experiment. Patterns A, B and C are used within the principal investigation while an optimization algorithm presented in Section 3.5 allows for determining groove pattern D. $w_G = 1.68$ is used instead of $w_G = 1.62$ due to geometric restrictions of the setup.

Parameter		Pattern			
	A	В	С	D	
Land width w_L [mm]	1.43	2.05	3.60	3.00	
Groove width W_G [mm]	0.80	1.15	2.00	1.68	
Open area [%]	35.9	35.9	35.9	35.9	

the network (El-Hosseiny 1990), we systematically varied the compression speed to investigate the effect of macroscale stress variations under different dynamic conditions. Following the approach of Wegele and Söderberg (2024), we applied ramp functions with varying load rates (1 MPa/s $\leq \dot{\sigma} \leq 1800$ MPa/s) and constant peak pressure ($\hat{\sigma} = 9$ MPa). As the press felt is a fibre system consisting of nonwoven layers, each experiment was repeated with three samples from the same press felt to obtain statistically reliable average data.

To describe the deformation behaviour of fibre networks, the modified strain δ_m is commonly used. It is defined as the logarithmic ratio of the porous network height h to the height h0 of a fully compacted (poreless) network:

$$\delta_m = \ln\left(\frac{h}{h_0}\right) = \ln\left(\frac{h \cdot \rho_f}{w}\right)$$
 (1)

Furthermore, the generated hydraulic pressure in the press felt is smaller than in the paper web as the pore size in the press felt is considerably higher (Moura et al. 2005; Wegele et al. 2024). Additionally, internal cohesion within the individual layers of the press felt created during the punch-needle process in the press felt manufacturing will prevent any stratification effects. Hence, the flow-generating work $W_{\it fl}$ does not need to be determined to evaluate the experiments.

2.3 Determination of mechanical stress variations

To evaluate if the setup allows for creating the macro-scale stress variations in the press felt, a pressure-sensitive film (Type Fuji Prescale LW) was placed on the top surface of a dry press felt prior to compression. The sample was then compressed against each groove pattern at $\dot{\sigma}=1$ MPa/s and $\hat{\sigma}=9$ MPa, creating a distribution of pixels of varying color intensity. The resulting imprint was analyzed using the correlation of colour intensity and pressure provided by the pressure-sensitive film manufacturer. As a result, the 2D mechanical pressure distribution $P_i(MD, CD)$ on the top surface of the press felt could be determined.

The imprints for the patterns A, B and C are shown in Figure 3 (see Appendix A for enlarged versions of the imprints). Macro-scale stress variations were observed for patterns B and C, with pattern C exhibiting the most pronounced variations. To allow a quantitative evaluation of this result, we average the pressure along the MD-axis for all recorded pixels, which aligns with the principal groove direction, calculating the respective CD stress profile $p_i(CD)$:

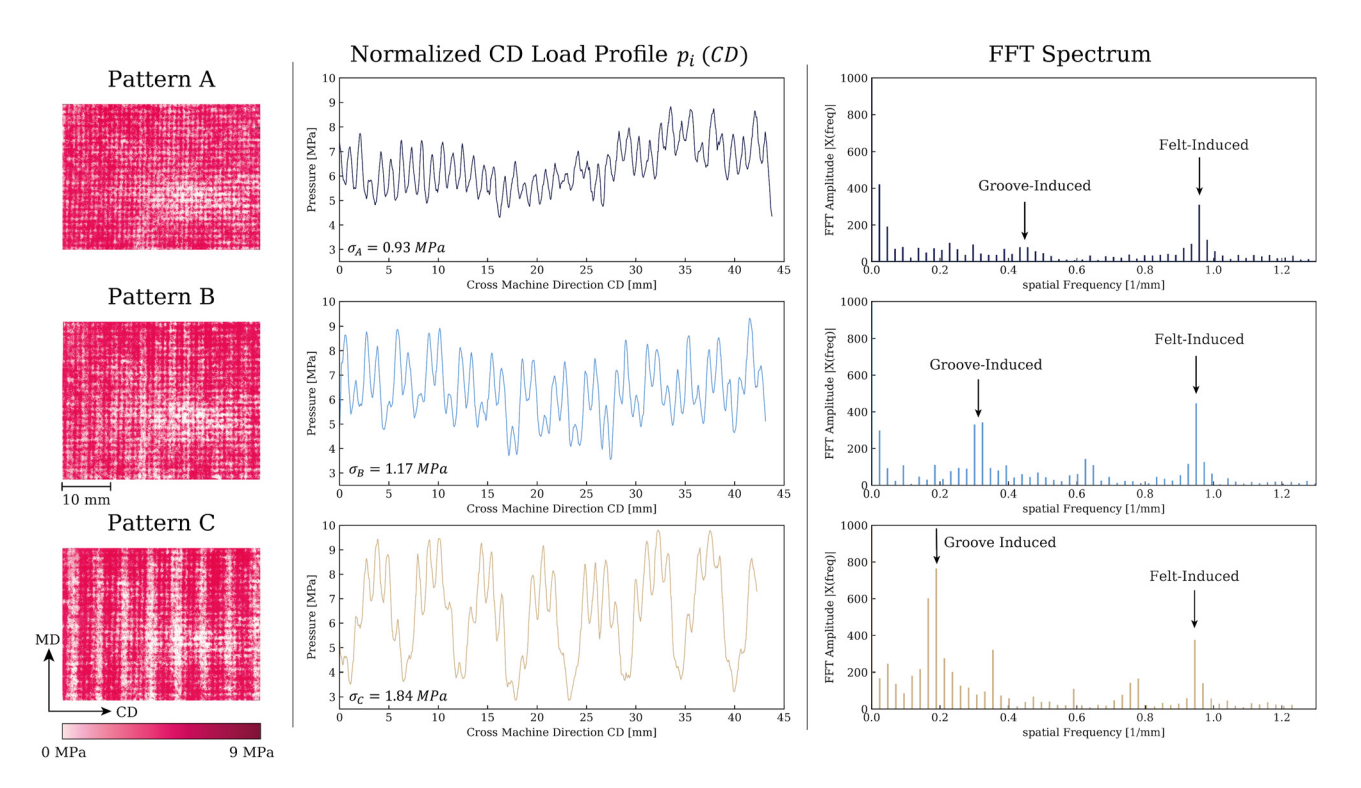


Figure 3: Left: Imprint results for the patterns A, B and C. Recorded at 24 °C and 60 % RH. Center: Normalized cross-directional (CD) stress profiles generated from calculating the mean stress value along the machine directional (MD) axis. Two different macro-scale stress signals are clearly visible. Hardly any groove induced macro-scale variations are visible for pattern A. Right: FFT analysis to quantify the amount of felt- and groove-induced macro-scale variations. As the geometries of the felt joints and groove inserts are known, the corresponding spatial frequency of the peaks can be determined.

$$p_i(CD) = \frac{1}{MD} \sum_{MD=1}^{MD} P_i(MD, CD)$$
 (2)

As the absolute peak pressure $\hat{\sigma}$ was not exactly constant within all conducted imprint experiments, we derive offset values to normalize the individual CD stress profiles to a reference profile. This was done by calculating the mean pressure $\overline{p_i}$ of the respective profiles along the CD-axis. Using $\overline{p_C}$ as a reference, the offset values Δp_A and Δp_B were determined by:

$$\Delta p_A = \overline{p_C} - \overline{p_A} \Delta p_B = \overline{p_C} - \overline{p_B}$$
 (3)

Using these offsets, the normalized CD stress profiles can be calculated by horizontally shifting the original profile $p_i(CD)$ with the offset values Δp_i :

$$p'_{A}(CD) = p_{A}(CD) + \Delta p_{A}$$

$$p'_{R}(CD) = p_{R}(CD) + \Delta p_{R}$$
(4)

The normalized CD stress profiles $p_i(CD)$ derived from the imprints confirm the presence of macro-scale stress variations of different extent, which can be differentiated in macro-scale stress variations created by the groove pattern and macro-scale stress variations created by structural joints within the woven base layer of the press felt. The groove-induced stress variations were most significant in pattern C, diminished in pattern B, and barely detectable in pattern A, where felt-induced stress variations dominated. To quantify the magnitude of the stress variations, the standard deviation σ_i of the individual CD stress profiles was calculated. The results indicate that pattern A exhibited an even pressure distribution (σ_A = 0.93 MPa), while the stress variations increased for pattern B (σ_B = 1.17 MPa) and were highest for pattern C (σ_C = 1.84 MPa). These findings demonstrate that total stress variations increase linearly with groove width w_G . Performing a Fast-Fourier-Transformation (FFT) on the CD load profiles allowed for quantifying and classifying the macro-scale variations, as visible in Figure 3. Peaks visible at a very low spatial frequencies are assigned to a lowpressure area also visible in all three imprints. This is caused by imperfections in the manufacturing of the impact body, leading to a slightly lower local compression load in this area. However, given that both the pattern geometries and felt joint spacing were known (see Table 1), the spatial frequencies of the groove- and felt-induced macro-scale stress variations were determined. This reveals that for pattern C, the groove-induced stress variations exceed the felt-induced stress variations with a distinct peak at 0.189 1/mm. The groove-induced stress variations are gradually reduced for pattern B and no longer visible for pattern A. This leads to the conclusion that no groove-induced stress variations are present on the top surface of the press felt when pattern A is used. However, felt-induced stress variations remain consistent across all patterns, with a frequency of approximately 0.95 1/mm. As a first conclusion, the setup allows for creating mechanical stress variations on the macro-scale of varying magnitude in press felt samples. This makes the setup a suitable tool to study the effect of macro-scale stress variations on the dynamic dewatering behaviour of saturated fibre networks.

3 Results and discussion

3.1 Groove entrance analysis

As the evaluation of the experiment relies on the measured modified strain, it is crucial to assess the loss in modified strain due to the fibre material being pressed into the grooves of the individual patterns. This effect was expected to be particularly pronounced for the coarser groove patterns B and C. Consequently, a press felt sample was compressed against a plain surface and the patterns B and C. Since no dewatering is possible using a plain counter surface, high hydraulic pressures would be generated, leading to an increased resistance for further compression. To eliminate this effect, the groove entrance experiments were conducted with press felt samples blown dry with pressurized air, removing free water from the fibre network while maintaining a lubricated fibre system. With this method, the overall compression resistance of the press felt is identical to the structural compression resistance of a saturated network as used in the dynamic dewatering experiments. Since press felts without free water do not exhibit any viscoelastic behaviour (El-Hosseiny 1990), the groove entrance experiments were conducted at one single load rate of $\dot{\sigma}$ = 90 MPa/s. The results of the groove entrance analysis experiments are depicted in Figure 4. The data indicate that considerably lower modified strains were observed when the press felt was compressed against grooved counter surfaces compared to the plain surface. These differences are significant, as a loss in the modified strain of $\Delta \delta_m$ = 0.08 is reached at σ = 8 MPa. Interestingly, there is no significant difference in the compression behaviour of the press felt samples when pressed against patterns B and C, which is only around $\Delta \delta_m$ = 0.005 at σ = 8 MPa. These findings suggest that a substantial amount of the fibrous material is being pressed into the

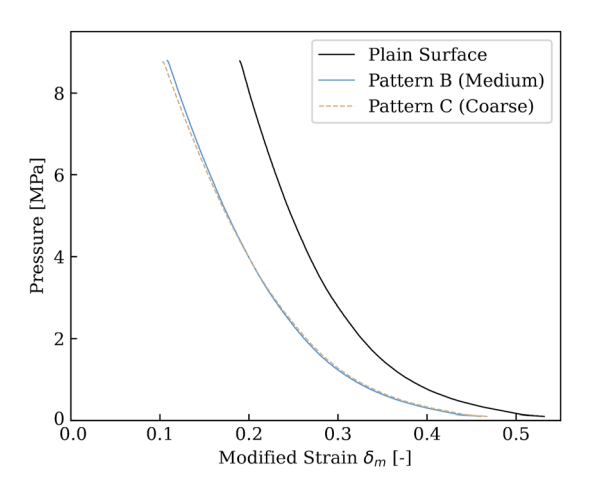


Figure 4: Stress-strain diagram for a lubricated press felt pressed against different surfaces (plain, pattern B and pattern C) at a load rate of $\dot{\sigma} = 90$ MPa/s. No significant differences in the compression properties between the grooved surfaces with identical open area can be detected.

grooves, but this amount remains consistent across patterns with identical open areas. This implies that groove width does not significantly influence the volume of fibres pressed into the grooves. In contrast to Vomhoff and Norman (2001), these results do not allow the calculation of the dryness of the network just by evaluating the modified strain. A significant volume of the water-containing press felt is pressed into the grooves, reducing the measured modified strain but not accounting for the network compression.

3.2 Stress-strain behaviour for different counter surfaces

The stress-strain behaviour of press felts has been frequently investigated in the past (e.g. El-Hosseiny 1990; Gustafsson and Kaul 2001; Hakala and Harlin 2008; Luciano 1983; Österberg 1988; Swain 1980). Therefore, our analysis focuses on the influence of the used groove pattern on the press felt compression at varying compression dynamics. The stress-strain diagrams of the press felt compressed against groove patterns A, B and C at different load rates $\dot{\sigma}_i$ are depicted in Figure 5. While no significant differences were observed when compressing the press felt against patterns A and C, lower modified strains could be reached using groove pattern B through the whole compression process. This was repeatable and observed for all investigated load rates. Referring to Table 2, pattern B reduced the minimum modified strain $\delta_{m, \min}$ by approximately $\Delta \delta_m =$ 0.016-0.009 compared to pattern A and $\Delta\delta_m$ = 0.014-0.008compared to pattern C at σ = 8 MPa. The average reduction in modified strain $\delta_{m,avg}$ achieved by using groove pattern B can be determined to be 0.012 compared to pattern A and 0.011 compared to pattern C. These findings indicate that the press felt compressibility is highest when compressed against groove pattern B. As no differences in the compression properties of press felts without free water in the pores could be determined (see Section 3.1), the observed differences in the compression behaviour must be attributed to macro-scale stress variations. These stress variations create an inhomogeneous porosity field within the press felt, influencing fluid flow within the network. Consequently, it is hypothesized that groove pattern B facilitates the highest dewatering efficiency, which requires an in-depth dewatering analysis.

Table 2: Overview on the minimum modified strains $\delta_{m, \min}$ reached at 8 MPa for different load rates and groove patterns A, B, C for experiments conducted with the identical press felt sample.

σ [MPa/s]	Min. δ_m at σ = 8 MPa				
	A	В	C		
1800	0.1189	0.1077	0.1214		
900	0.1179	0.1087	0.1166		
450	0.1227	0.1122	0.1231		
90	0.1212	0.1091	0.1219		
18	0.1223	0.1065	0.1182		
1	0.1128	0.0983	0.1098		

3.3 Felt dewatering analysis

In addition to evaluating the stress-strain behaviour of the press felt compressed against different groove patterns, the dewatering of the press felt was measured after every experiment and plotted as a function of the applied load rate $\dot{\sigma}$. To account for minor variations in the applied peak pressure $\hat{\sigma}$ caused by the control unit of the servo-hydraulic testing machine, the experimental data for each groove pattern is subjected to box filtering to remove individual outliers. The results are depicted in Figure 6. Given that the data typically exhibit some scattering, a third-order polynomial fit was used to describe the dewatering as a function of the applied load rate $\dot{\sigma}$ (see Appendix B for the determined

parameters of the fit). The results show that for all three groove patterns, high dewatering values of up to $80-100 \text{ g/m}^2$ are reached for quasi-static conditions at $\dot{\sigma} \leq 1$ MPa/s. This is explained with a sufficient dwell time, allowing the water to flow out of the compressed network at low flow velocity. Consequently, the resulting 2D permeability field of the inhomogeneously compressed network does not impede its water discharge. With increasing load rate, higher hydraulic pressures are generated within the network and macro-scale stress variations seem to alter the dewatering behaviour. In cases where the macro-scale stress variations created open flow paths at the same time with a homogeneous overall compression, the dewatering performance can increase with increasing load rate, causing a non-monotonous dewatering

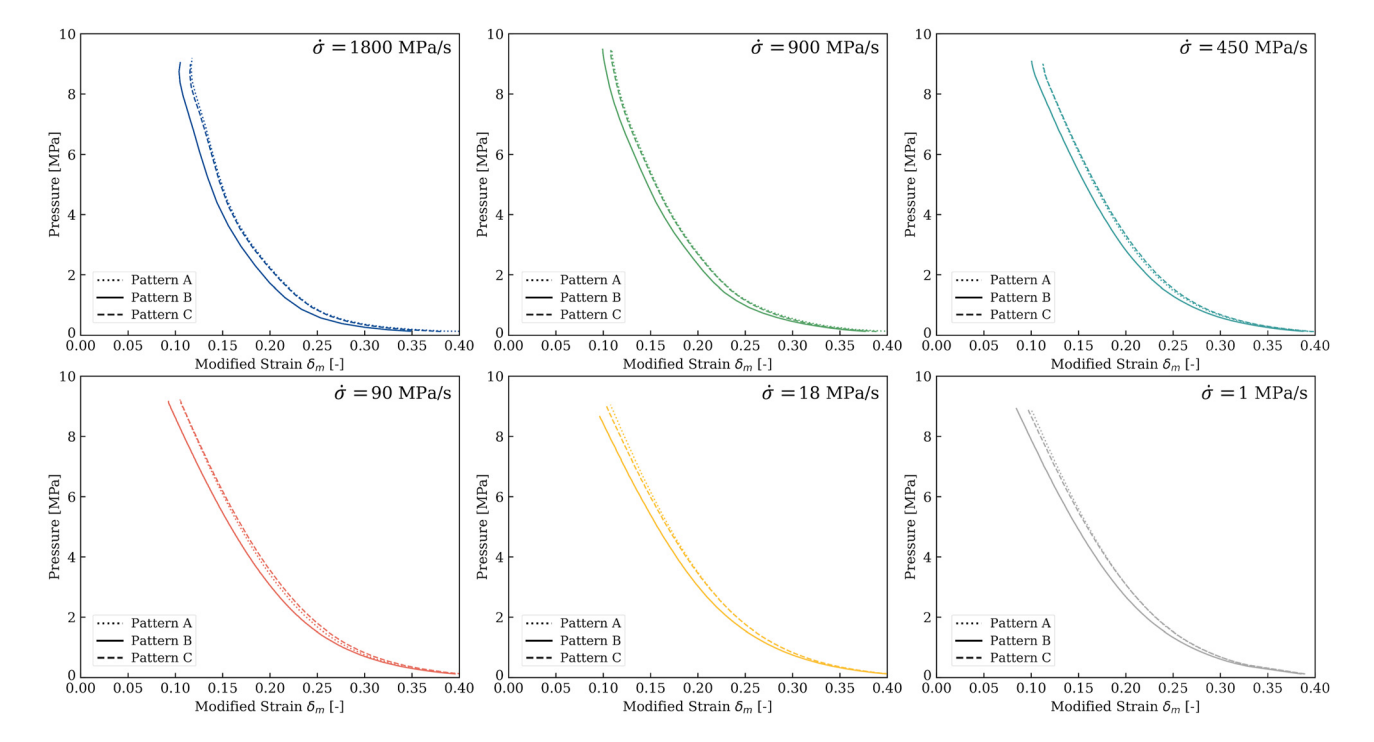


Figure 5: Direct comparison of the stress-strain behaviour of press felts pressed against different groove patterns in a range of load rates of $1 \le \dot{\sigma} \le 1800$ MPa/s.

behaviour. This effect has a clear dependence on the compression dynamics. While for $\dot{\sigma}$ = 500 MPa/s the dewatering values are still within the same range (pattern A: 53 g/ m², pattern B: 47 g/m², pattern C: 44 g/m²), the dewatering of pattern B increased to around 85 g/m² at $\dot{\sigma}$ = 1,500 MPa/s, exceeding the dewatering values by 27 g/m² for pattern A and 41 g/m² for pattern C. Across the full range of industrial relevant load rates (750 MPa/s $<\dot{\sigma}<$ 2000 MPa/s), the specific dewatering for groove pattern B exceeds the specific dewatering obtained with patterns A and C. However, the steep decline at load rates $\dot{\sigma}$ > 2000 MPa/s might not be physical but more a consequence of the curve fit. Referring to Section 2.3, the grooves in pattern A did not induce macro-scale stress variations, whereas the grooves in pattern C exhibited significant macro-scale stress variations, surpassing stress variations created by the felt joints. Pattern B, however, produced both groove- and felt-induced stress variations of similar magnitude. Since pattern B demonstrated the highest dewatering efficiency in the industrially relevant range, it is concluded that macro-scale stress variations induced by structured roll covers influenced the overall dewatering performance with increasing dynamics in the nip. To a certain extent, groove-induced macro-scale stress variations enhance the dewatering performance by improving the overall permeability of the network. However, excessive macro-scale stress variations negatively impact the dewatering efficiency due to inhomogeneous compression and elongated flow paths within the fiber network. Therefore, an optimal balance likely exists, where sufficient macro-scale stress variations promote open flow paths for high permeability while maintaining a homogeneous load distribution. To investigate this effect

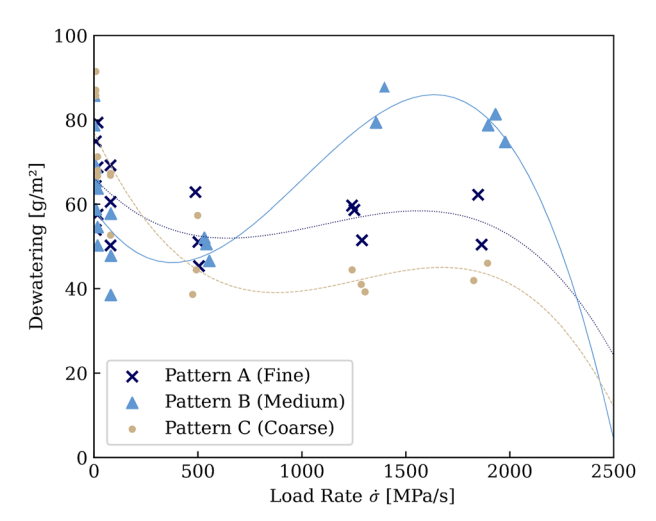


Figure 6: Press felt dewatering in g/m² for groove patterns A, B and C as a function of the applied load rate $\dot{\sigma}$. A polynomial function of 3rd order was used to fit the data.

further, a detailed analysis of the average flow speed within the fibre network is conducted in the following section.

3.4 Flow velocity calculations

Within our experiment, a saturated fibre network is compressed against a rigid grooved pattern, as depicted in Figure 7. While the overall area of the press felt is denoted with A, the open area of the groove pattern is denoted with A_0 . To calculate the average the z-directional flow velocity $\bar{v}_z(t)$ at the interface of the press felt to the groove section, it is assumed that the overall reduction in volume of the press felt equals the displaced water volume, which is valid for saturated conditions. Using the displacement data recorded by the eddy-current sensors during compression experiments allows for calculating the volumetric flow rate $\dot{V}(t)$ by taking into account the area $A = w \cdot d$ of the press felt specimen:

$$\dot{V}(t) = \frac{\mathrm{d}h}{\mathrm{d}t} \cdot A \tag{5}$$

This allows for a calculation of the superficial velocity $q_z(t)$ just above the groove pattern, assuming that all displaced liquid volume needs to be pressed into the grooves through the open area A_0 .

$$q_z(t) = \frac{\dot{V}(t)}{A_0} \tag{6}$$

As the network is consolidating, the porosity is gradually reduced, causing a restriction of the available area for the water to flow out of the network. Using the block height h_0 as reference, the porosity $\phi(t)$ can be expressed as a function of the network height h(t):

$$\phi(t) = \frac{h(t) - h_0}{h(t)} = \frac{h(t) - (w_f / \rho_f)}{h(t)}$$
(7)

With the simplifying assumption, that the porosity $\phi(t)$ is homogeneously distributed across the whole press felt, $\overline{v_z}$ (t) is calculated:

$$\overline{v_z}(t) = \frac{q_z(t)}{\phi(t)} \tag{8}$$

Applying this calculation to the experimental data allows for plotting the average z-directional flow velocity as a function of the modified strain for different groove patterns, as shown in Figure 8. The results indicate that dewatering velocity decreases with decreasing load rate. At high load rates ($\dot{\sigma} > 450$ MPa/s), the dewatering velocity increases at the beginning of the compression, reaching a plateau before gradually decreasing towards the end of the

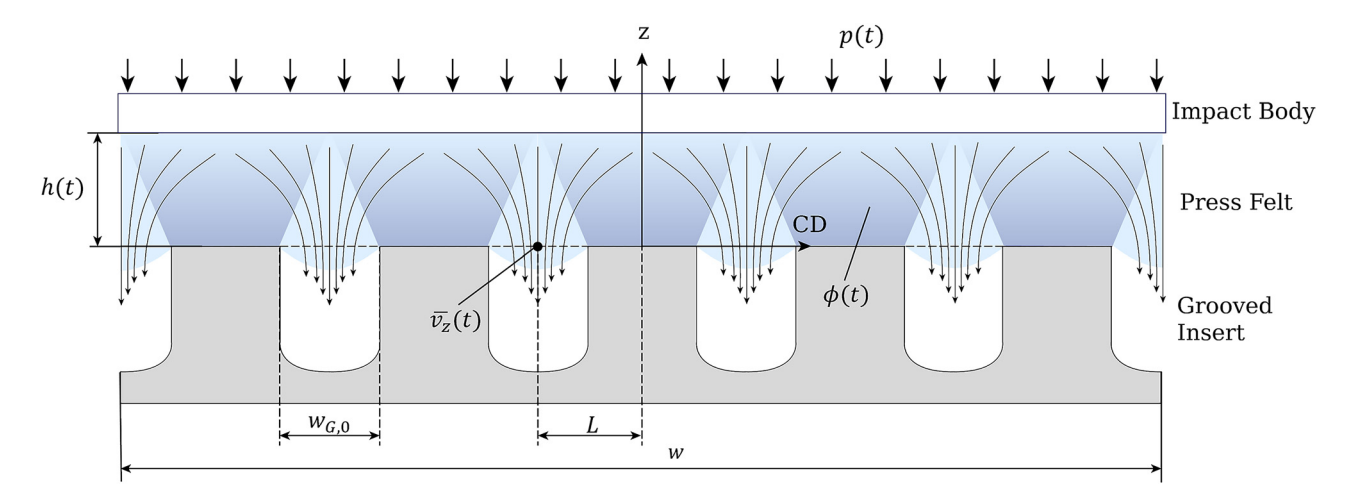


Figure 7: Experimental situation for calculating the average *z*-directional velocity $\overline{v_z}(t)$, which is assumed to be present just above the grooves as denoted in the figure. The average flow path is assumed to be $L = (w_G + w_I)/2$.

compression at low modified strains. In contrast, at low load rates ($\dot{\sigma}$ < 100 MPa/s), the dewatering velocity exhibits a peak at high modified strains, followed by a gradual decline as the compression progresses. A comparison of dewatering velocities at identical load rates across different groove patterns reveals that groove pattern B consistently achieves higher dewatering velocities compared to patterns A and C. This trend is observed across all load rates, although the differences diminish as load rates decrease.

To evaluate these results, the theoretical correlation for the single-phase flow through a porous network is derived. As Darcy's law is limited to creeping flows, the Forchheimer approximation (Forchheimer 1901) should be used as it also encounters pressure losses due to turbulent dissipation:

$$\Delta p = \frac{\mu v_z}{k} + \beta \rho v_z^2 \tag{9}$$

However, this results in a nonlinear correlation of pressure and flow with the additional problem of different permeabilities k and β , which usually are experimentally determined. Therefore, we are using Darcy's law to interpret the flow velocity calculation results as its linearity in the relation of pressure and flow velocity allows for getting a reasonable understanding of the underlying effects when the press felt is compressed against grooved structures. Furthermore, previous experiments on press felts show the validity of using Darcy's law to describe the flow through saturated press felts (Thibault and Bloch 2008; Thibault et al. 2001). Darcy's law can be written as:

$$\mathbf{q} = -\frac{k}{\mu} \nabla p \tag{10}$$

In the equation, ∇p is the hydraulic gradient, \mathbf{q} the Darcy flux which corresponds to the superficial velocity and $-\frac{k}{u}$ the

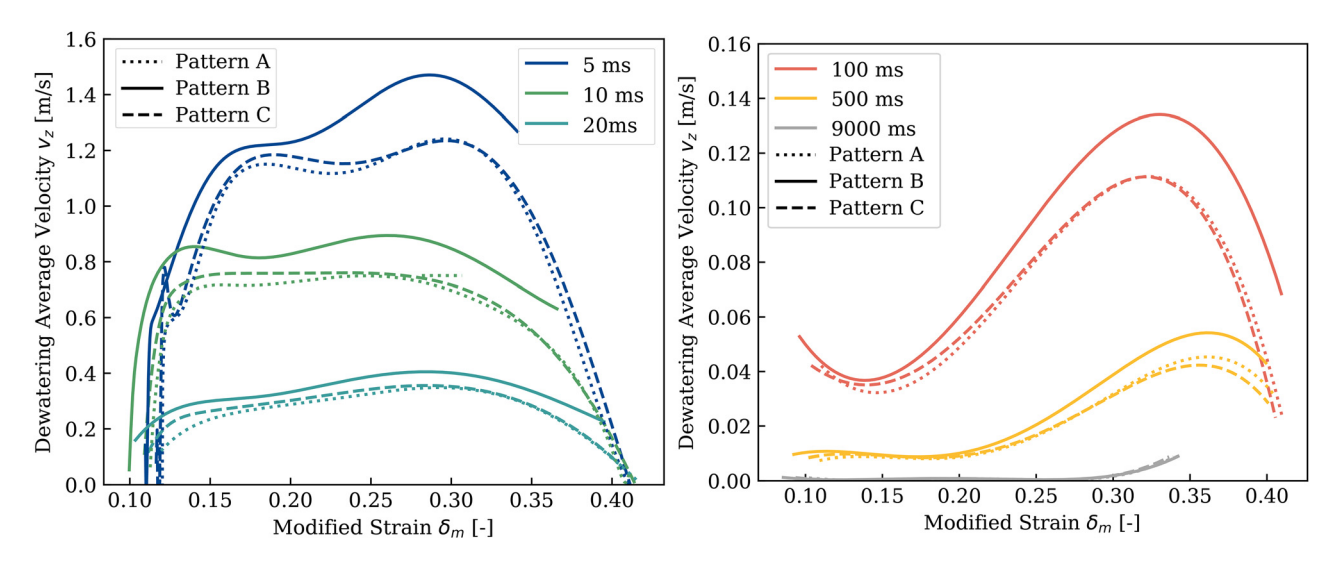


Figure 8: Calculated average *z*-directional flow velocity as a function of the modified strain for different groove patterns and load rates. Attention: the scale on the diagram on the right for the low load rates has different *y*-axis scaling.

hydraulic conductivity. In the integral form, the hydraulic gradient corresponds to the pressure drop between the top surface of the press felt and the grooved section Δp and the flow path L:

$$\nabla p = \frac{\Delta p}{L} = \frac{p_1 - p_0}{L} \tag{11}$$

Considering Eq. (8) allows to formulate a correlation for the z-directional average flow velocity v_z :

$$v_z = -\frac{k}{\mu L} \cdot \Delta p \cdot \frac{1}{\phi} \tag{12}$$

As the porosity is a function of the compression state of the network (see Eq. (7)) and the pressure gradient along the principal flow direction is assumed to depend on the load rate of the compression process, the average dewatering velocity for identical load rates at fixed applied pressure and viscosity is proportional to the permeability of the network and the flow path, hence:

$$v_z \propto \frac{k}{L}$$
 (13)

This reveals that high network discharge is reached when the ratio of permeability and flow length is maximized. As the observed increase in dewatering for groove pattern B coincides with high flow velocities, we conclude that groove pattern B creates macro-scale stress variations that lead to a higher k/L ratio for patterns A and C. To further optimize the press felt and roll cover interactions, we therefore propose the following condition:

$$\max\left(\frac{k}{L}\right) \tag{14}$$

as an optimization criteria that provides maximized press felt dewatering. Since the permeability of the press felt is always a result of the felt internal structure, the optimized counter surface is highly felt-specific and will differ for different press felts. For our specific case, a multivariate regression analysis of the experimental data is applied in the following, presenting a possible approach to determine the optimized groove pattern that will provide the highest press felt dewatering performance.

3.5 Optimization algorithm

In the following, we present an optimization strategy using a multivariate polynomial regression method applied on the dewatering results to determine a groove pattern creating optimised macro-scale stress variations in the press felt to provide maximized felt dewatering. A constant open area of the groove pattern is set as a boundary condition, allowing us to use the groove width w_G as a groove pattern classifier.

The dewatering y of the press felt is modeled as a polynomial function f of the load rate $\dot{\sigma}$ and groove width w_G with the error ε :

$$y = f(\dot{\sigma}, w_G) + \varepsilon \tag{15}$$

Using the function grade k, we create monomials in the form $\dot{\sigma}^a$, w_G^b , with the condition of $a + b \le k$ and $a, b \ge 0$. For nindividual dewatering experiments, the design matrix X can be defined, having the shape of $n \times t$ with t being:

$$t = \frac{(k+2)(k+1)}{2} \tag{16}$$

With n dewatering results used as a $n \times 1$ -shaped response vector \overrightarrow{y} , we can set up the multivariate polynomial regression model in matrix notation introducing the parameter vector $\overrightarrow{\beta}$ and the vector of random errors $\overrightarrow{\varepsilon}$:

$$\vec{y} = \mathbf{X}\vec{\boldsymbol{\beta}} + \vec{\boldsymbol{\varepsilon}} \tag{17}$$

The algorithm was iteratively applied with polynomial functions of increasing degree k_i until the root mean squared error (RMSE) of the fit increased to determine the optimal polynomial order for the regression model. The optimal degree k used for the groove pattern optimization can be determined as k_{i-1} . Figure 9a illustrates this procedure applied to the dataset, demonstrating that a fifth-order polynomial (k = 5) provides the lowest RMSE and, therefore, the most accurate prediction. The optimized regression function, shown in Figure 9b, predicts a global maximum for press felt dewatering at a groove width of w_G = 1.62 mm and a load rate of $\dot{\sigma}$ = 1978 MPa/s. As observed in Section 3.3 the groove pattern has an increasing influence on the press felt dewatering with increasing load rate. Consequently, the predicted maximum aligns with expectations and will be experimentally validated in the following section.

3.6 Verification of optimization

To validate the optimization results, an additional groove pattern D was manufactured based on the predicted dimensions of the regression model and the dewatering experiments were repeated using a new set of samples from the same press felt. Given that the predicted dewatering maximum was identified at $\dot{\sigma} = 1980 \,\mathrm{MPa/s}$, additional high-speed compression tests were performed, providing a broader dataset in the industrially relevant range of load

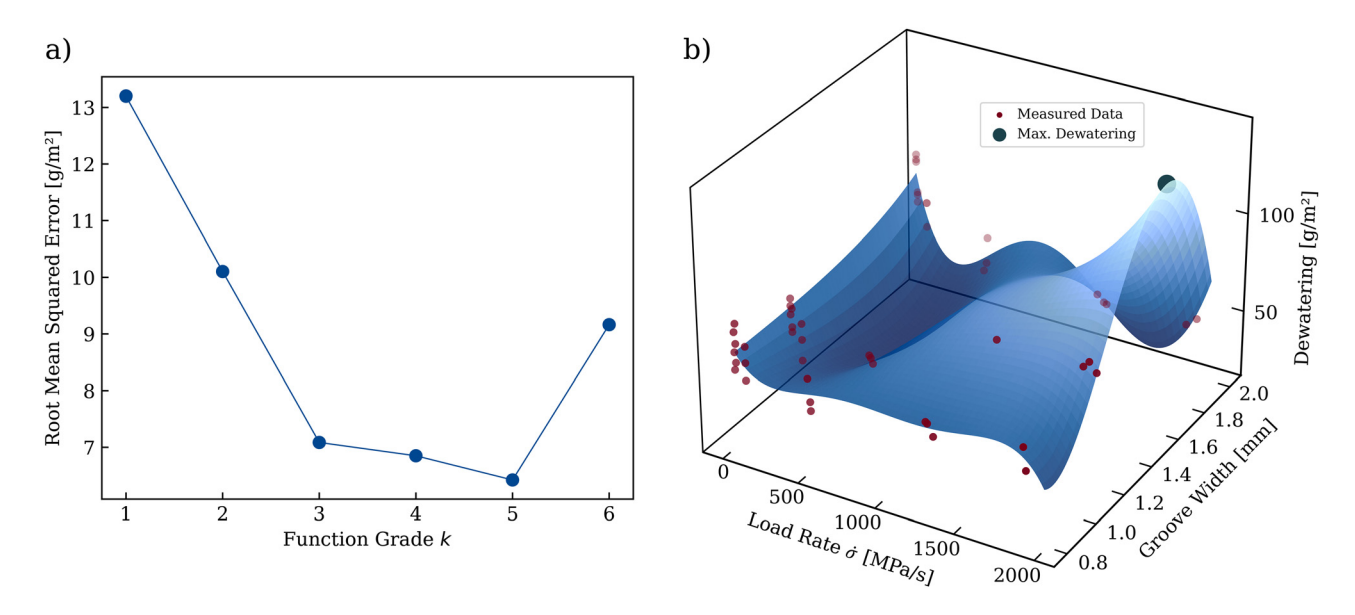


Figure 9: Results of the optimization algorithm. (a) Root mean squared error for fitting the dataset **X** to polynomial functions of function grade k. A polynomial function of grade k = 5 will provide results with the lowest mean squared error of around 6.4 g/m^2 . (b) Predicted dewatering data as a surface plot for load rates and groove patterns within the parameter space. The data points from the design matrix **X** are depicted in red while the determined dewatering optimum is depicted as green point.

rates. Again, a box filter was applied to remove outliers in the peak pressure signal from the raw datasets of the individual groove patterns. The results of the verification experiments are depicted in Figure 10. When comparing the optimized pattern D with patterns B and C, slightly lower dewatering values were observed at low to medium load rates $\dot{\sigma} < 900$ MPa/s. Starting at $\dot{\sigma} = 500$ MPa/s, the dewatering of groove pattern C starts to remain at a range

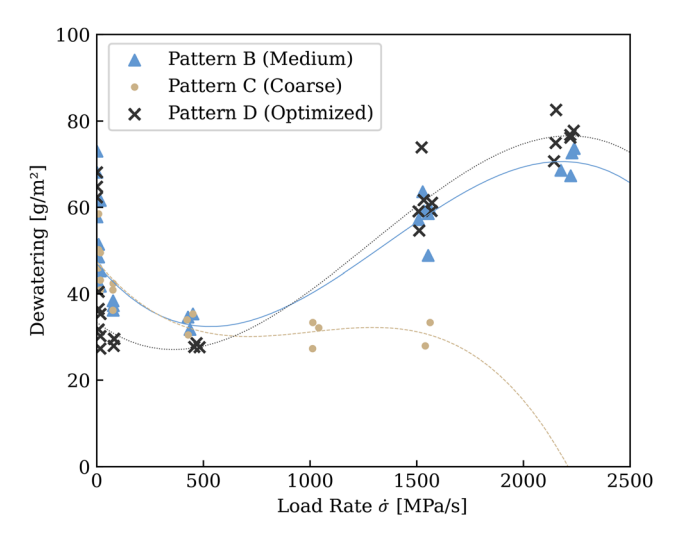


Figure 10: The result of the verification experiment. The dewatering of the press felt used with the optimized groove pattern is increased for load rates higher than $\dot{\sigma}$ = 1800 MPa/s. The differences in the individual dewatering behaviour in the main and verification experiments for patterns B and C are explained with variations in the sample structure, as for the verification experiments, a new set of samples was used.

of 30 g/m² while patterns B and C show an increase to around 60 g/m² at $\dot{\sigma}=1,520$ MPa/s. At higher load rates ($\dot{\sigma}>1,515$ MPa/s), the optimized pattern D consistently outperformed pattern B, demonstrating a clear increase in dewatering efficiency. Referring to the applied fit of a polynomial function of 3rd order, the increase was determined in the range of 7.3 % for a load rate of $\dot{\sigma}=2000$ MPa/s. These findings confirm that the optimization algorithm successfully identified a groove geometry that enhances press felt dewatering performance under highly dynamic nip conditions, as encountered in industrial paper machines.

4 Conclusions

The experimental setup developed in this study successfully generates macro-scale stress variations of varying intensities in a press felt. Combined with eddy-current sensors and a load cell, the system enables a comprehensive evaluation of experimental results, considering both water removal and dynamically recorded stress-strain profiles.

When pressed against groove patterns with identical open areas but different groove and land widths, significant differences in the compression behaviour of saturated press felts could be detected. Since these differences could not be observed when no flow was created in the press felt, it can be concluded that macro-scale stress variations are related to hydraulic effects, significantly influencing both the compression and dewatering performance once saturation

is reached. Furthermore, as nip dynamics increase, the influence of the groove pattern becomes more pronounced, confirming that hydraulic pressure contributions play a key role in fiber network compression. The lower modified strain reached for experiments conducted with groove pattern B coincided with high press felt dewatering results obtained with the same groove pattern at load rates higher than 750 MPa/s. Hence, higher network compressibility renders high dewatering values for highly dynamic applications. By providing local macro-scale stress variations, highly permeable areas in the press felt are maintained during the compression, which assists the network discharge by allowing an increased z-directional network permeability. However, these effects are limited once the grooves create highly uncompressed felt areas, limiting the overall dewatering efficiency. Further analysis revealed that the highest average flow velocities at identical load rates were achieved with groove pattern B. A comparison with the Darcy equation suggests that optimizing the k/L-ratio is essential for maximizing the dewatering efficiency. While macro-scale stress variations can enhance the overall permeability, excessively long flow paths L can counteract these benefits. To optimize this k/L-ratio for our specific case, we applied a multivariate polynomial regression method to determine the optimized groove width based on the recorded dewatering data. Repeating the dewatering experiments with the optimized groove pattern showed an increase in press felt dewatering of around 7% for a highly dynamic situation. Hence, our method allows us to determine a groove pattern that shows optimized dewatering performance for a specific press felt when operating under saturated conditions, which are usually present when nip dewatering is facilitated. Given that nip dewatering is generally pursued nowadays, large volumes of water are present in the press felt, creating a saturated system even in the early stages of the nip impulse. Therefore, it is crucial to achieve optimal flow conditions under saturation to provide a more efficient nip dewatering. The method described in this study allows for optimizing the

groove surfaces of press rolls for a specific press felt, resulting in increased dewatering performance due to higher felt permeability. Consequently, this method is a valuable tool for further optimizing the press nip and creating customized systems based on specific boundary conditions like peak pressure, nip dynamics and water volumes.

Acknowledgments: The authors would like to thank Dr. Helga Krieger and Timo Frick for the fruitful discussions that lead to this study. Simon Ermert and Richard Westerholz are thanked for their support within the experimental part of the underlying work. Jana Roth is thanked for her support with optimizing the groove pattern geometry.

Research ethics: Not applicable.

Informed consent: Informed consent was obtained from all individuals included in this study, or their legal guardians or wards.

Author contributions: All authors have accepted responsibility for the entire content of this manuscript and approved its submission.

Use of Large Language Models, AI and Machine Learning Tools: None declared.

Conflict of interest: Patrick Wegele reports financial support and equipment were provided by J.M. Voith SE & Co. KG. Patrick Wegele reports a relationship with J.M. Voith SE & Co. KG, including employment. L. Daniel Söderberg declares no conflict of interest.

Research funding: The Knut and Alice Wallenberg Foundation is acknowledged for funding Daniel Söderberg through the Wallenberg Wood Science Center.

Data availability: The raw data can be obtained on request from the corresponding author.

Appendix A: Enlarged imprints of the static pressure distribution

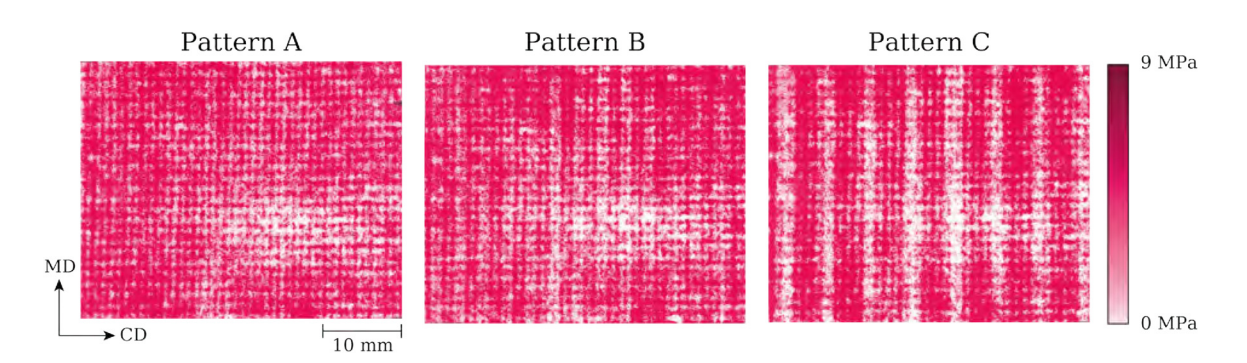


Figure A.11: Enlarged image of the imprints recorded during experiments in Section 2.3. While the felt-induced stress variations are clearly visible as individual dots, the groove-induced stress variations can be identified as vertical stripes.

Appendix B: Results dewatering data fit

Table B.3: Results of the fit of the dewatering data to a polynomial function of 3rd order. Sample set 1 is used for the initial dewatering experiments in Section 3.3. Sample set 2 is used during the verification experiments of the optimization in Section 3.5.

Set of	Pattern	Parameter				R ²
samples		а	b	С	d	
1	Α	$-1.68 \cdot 10^{-8}$	5.58 · 10 ⁻⁵	5.09 · 10 ⁻²	66.16	0.31
	В	$-3.98 \cdot 10^{-8}$	$1.20 \cdot 10^{-4}$	$-7.36 \cdot 10^{-2}$	58.96	0.77
	C	$-2.39 \cdot 10^{-8}$	$9.13 \cdot 10^{5}$	$-1.05 \cdot 10^{-1}$	77.04	0.78
2	В	$-1.71 \cdot 10^{-8}$	$6.96 \cdot 10^{-5}$	$-5.95 \cdot 10^{-2}$	46.93	0.85
	C	$-2.15 \cdot 10^{-8}$	$6.48 \cdot 10^{-5}$	$-5.96 \cdot 10^{-2}$	47.47	0.74
	D	$-1.55 \cdot 10^{-8}$	$5.98 \cdot 10^{-5}$	$-3.70 \cdot 10^{-2}$	33.38	0.96

References

- Armstrong, T. (2005). Advances in shoe press sleeves. In: Proceedings from the 2005 TAPPI papermakers and PIMA international leadership conference, Milwaukee, WI, pp. 791-809.
- Ballard, J. (1986). Press felt characterization. In: Proceedings from the 1986 TAPPI engineering conference, Atlanta, GA, pp. 117-122.
- Chevallier, P. (1992). Felt design factor: a tool for optimizing sheet dryness. In: Proceedings from the 1992 TAPPI engineering conference, Boston, MA, pp. 877-898.
- El-Hosseiny, F. (1990). Compression behavior of press felts and wet webs. Nord. Pulp Pap. Res. J. 5: 28-32, https://doi.org/10.3183/npprj-1990-05-
- Fekete, E. (1975). Water removal performance on a grooved second press, part 2: stratified felts. Pap. Technol. Ind. 16: 117-181.
- Forchheimer, P. (1901). Wasserbewegung durch boden. Zeit. Verl. Deut. Ing. 45: 1782-1788.
- Gullbrand, J. and Vomhoff, H. (2003). A new method for the characterisation of micro-scale stress variations of press felts. Nord. Pulp Pap. Res. J. 18: 18-23, https://doi.org/10.3183/npprj-2003-18-01-p018-023.
- Gullbrand, J. and Vomhoff, H. (2005). The influence of press felt micro-scale stress variation on dewatering. Nord. Pulp Pap. Res. J. 20: 289-297, https://doi.org/10.3183/npprj-2005-20-03-p289-297.
- Gustafsson, J.E. and Kaul, V. (2001). A general model of deformation and flow in wet fibre webs under compression. Nord. Pulp Pap. Res. J. 16: 149-155, https://doi.org/10.3183/npprj-2001-16-02p149-155.
- Hakala, T. and Harlin, A. (2008). Simulation of a rapid nip pressure strike and its effect on press felt samples. Autex Res. J. 8: 84-91, https://doi.org/ 10.1515/aut-2008-080305.
- Kershaw, T.N. (1972). The three dimensions of water flow in press felts. TAPPI 55: 880-887.

- l'Anson, S. and Ashwort, T. (2000). Differentiated-permeability surface layer (dpsl) pressing theory. TAPPI J. 83.
- Luciano, W. (1983). Practical model for felt compressibility. J. Pulp Pap. Sci. 9: 65-68.
- MacGregor, M.A. (1989) Wet pressing research in 1989 an historical perspective, analysis, and commentary. In: Fundamentals of papermaking, trans. of the XIth fund. res. symp. Cambridge, pp. 511–586.
- Machlem, J.E. (1961). A study of the resistance of woven wool felts to liquid flow. TAPPI 44: 535-544.
- McDonald, J. and Pikulik, I. (1992) Felt construction and water removal in a press nip. In: Proceedings from the 1992 TAPPI engineering conference, Boston, MA, pp. 869-876.
- McDonald, D., Pikulik, I., Ko, P., and Owston, T. (2002). Optimizing market pulp felt design for water removal. J. Pulp Pap. Sci. 28: 17-22.
- Moura, M., Ferreira, P., and Figueiredo, M. (2005). Mercury intrusion porosimetry in pulp and paper technology. Powder Technol. 160: 61-66, https://doi.org/10.1016/j.powtec.2005.08.033.
- Oliver, J. and Wiseman, N. (1977) Significance of felt roughness in wet pressing. In: Trans. of the VIth fund. res. symp. Oxford, pp. 411-417.
- Österberg, L.B. (1988). Compression of press felts. Nord. Pulp Pap. Res. J. 3:
- Skelton, J. and Toney, M. (1998) Modeling of press fabrics and vented press belts for shoe presses. In: Proceedings of the 1998 TAPPI international engineering conference, Atlanta, GA, pp. 553-556.
- Swain, G.E. (1980). Behavior of press felts in compression. TAPPI 63: 85–88. Sze, D.H. (1986). Measuring wet press felt pressure uniformity and its effect on sheet solids. Tappi J. 4: 120-124.
- Thibault, X. and Bloch, J.F. (2008). Permeability measurements of strained fibrous networks. Text. Res. J. 78: 473-485, https://doi.org/10.1177/ 0040517507081912.
- Thibault, X., Bloch, J.F., Chave, Y., and Serra-Tosio, J.M. (2001) Permeability measurements of press felts. In: Trans. of the XIIth fund. res. symp. Oxford, pp. 947-974.
- Vomhoff, H. (2000). On the in-plane permeability of water-saturated fibre webs. Nord. Pulp Pap. Res. J. 15: 200-204, https://doi.org/10.3183/ nppri-2000-15-03-p200-204.
- Vomhoff, H. and Norman, B. (1997). Model experiments on wet pressing – the influence of felt surface structure. Nord. Pulp Pap. Res. J. 12: 54-60, https://doi.org/10.3183/npprj-1997-12-01-p054-060.
- Vomhoff, H. and Norman, B. (2001). Method for the investigation of the dynamic compressibility of wet fibre networks. Nord. Pulp Pap. Res. J. 16: 57-62, https://doi.org/10.3183/npprj-2001-16-01-p057-062.
- Wegele, P. and Söderberg, L.D. (2024). Experimental method for investigating the dynamic compression behaviour of fibre-reinforced polyurethane shoe press belts under press nip conditions. Compos., Part C 14: 100476, https://doi.org/10.1016/j.jcomc.2024.100476.
- Wegele, P., Rosén, T., and Söderberg, L.D. (2024). Multiphase distribution in partly saturated hierarchical nonwoven fibre networks under applied load using x-ray computed tomography. Exp. Fluids 65: 140, https:// doi.org/10.1007/s00348-024-03869-y.
- Xu, J., Phillip, R., and Hedou, D. (2011) The effect of press felt non-uniformity on sheet smoothness and dewatering. In: Proceedings from the paper conference and trade show 2011, Covington, KY, pp. 1121–1126.
- Xu, J., Foisy, L., and Hedou, D. (2013) A study of the interaction between shoe press sleeves and press fabrics. In: Proceedings from the paper conference and trade show 2013, Atlanta, GA, pp. 854-871.